ent from other southwest sites and reflect the distinctive geology of the area. The presence of crystal quartz indicates contact with Bone Cave and the Weld River, 25 km to the south where deposits of the material are known (*5*).

Five pieces of the impactite, Darwin glass (*10*), were excavated from the deposits, the lowest being associated with a date of ~27,770 BP. It suggests contact with the Darwin meteorite crater 75 km to the west. A journey of over 100 km down the principal river systems would have been involved in bringing this stone into the Florentine valley. Its appearance at Bluff Cave predates its introduction into Kutikina Cave by 10,000 years. The presence of the distinctive raw materials and tool types at Bluff Cave links it into a network of human activity centered on southwest Tasmania during the Pleistocene.

No common southwest raw materials such as chert, crystal, and milky quartz or Darwin glass were excavated from site ORS 7. The majority of stone raw materials excavated are locally available. In addition, no thumbnail scrapers were recorded from ORS 7. Although alkaline soil conditions occur at both sites, the amount of faunal remains preserved at each is significantly different. The distinct pattern of late Pleistocene artifact assemblages, raw materials, and fauna found between the southwest and southeast regions suggest adaptations to distinctive, but related environments.

These results are important in three ways. First, they push back the timing of human colonization of Tasmania at least 8,000 years; second, they indicate human exploitation of upland environments 10,000 years earlier than previously recorded on the Australian mainland (*11, 12*) and 20,000 years earlier in Tasmania (*13*); and third, they suggest that by 30,000 years ago megafauna was extinct in Tasmania. The first is significant in light of the recent evidence for sea level fluctuations in the Bass Strait area between 55,000 and 10,000 years ago (*14–16*). These data suggest three periods prior to the onset of the last glacial (25,000 to 10,000 years ago) when Tasmania was connected to the Australian mainland by the exposed Bassian Rise, the longest extending from 37,000 to 29,000 years ago. This approximates the oldest secure date for human occupation in Greater Australia (40,000 years) from eastern New Guinea (*17*). The possibility now arises that humans reached Tasmania 36,000 years ago when a drop in sea level of 55 m exposed a portion of the Bassian Rise.

The second import of the dates is that although Pleistocene human presence in central Tasmania had been previously demonstrated (*6*), the new data indicate occupation of the southern edge of the flat, exposed highlands prior to, and during the height of, the last glacial period. This area carried the largest Tasmanian ice sheet 18,000 years ago. It suggests that people were less concerned with extreme climatic conditions and more intent on the systematic exploitation of a range of environments economically important to them.

The absence of extinct fauna at both sites raises questions about evidence from the Florentine valley suggesting the coexistence of humans and megafauna 20,000 years ago (*6*). An earlier notion that these animals became extinct 11,000 years ago due to vegetational changes is not supported by the present data (*18*). Although specialized kill and consumption sites away from rockshelters cannot be ruled out, the evidence points to an early extinction of these animals prior to human arrival in south central Tasmania. The data further indicate that at this stage of colonization, people were not limited to a narrow littoral and marine economy (*19, 20*) but were focusing on inland environmental zones, hunting a range of modern terrestrial fauna.

REFERENCES AND NOTES

1. H. Lourandos, in *Prehistoric Hunter Gatherers*, T. D. Price and J. A. Brown, Eds. (Academic Press, New York, 1985), pp. 385–424.
2. D. Horton, in *The Pleistocene Perspective* (Allen & Unwin, London, 1986), vol. 2, pp. 1–14.
3. P. J. White and J. F. O'Connell, *A Prehistory of Australia, New Guinea and Sahul* (Academic Press, Sydney, 1982).
4. K. Kiernan, R. Jones, D. Ranson, *Nature* **301**, 28 (1983).
5. J. Allen, R. Cosgrove, S. Brown, *Australian Archaeol.*, in press.
6. P. Murray, A. Goede, J. L. Bada, *Archaeol. Phys. Anthropol. Oceania* **15**, 142 (1980).
7. T. Watkins, Ed., *Radiocarbon: Calibration and Prehistory* (Edinburgh Univ. Press, Edinburgh, 1975).
8. A. Goede and P. Murray, *Mankind* **11**, 2 (1977).
9. R. Jones and J. Allen, *Australian Archaeol.* **19**, 86 (1984).
10. R. F. Fudali and R. J. Ford, *Meteoritics* **14**, 283 (1979).
11. S. Bowdler, *Archaeol. Oceania* **16**, 99 (1981).
12. J. Flood, B. David, J. Magee, B. English, *ibid.* **22**, 9 (1986).
13. H. Lourandos, *Australian Archaeol.* **16**, 39 (1983).
14. W. M. Blom, *Search* **19**, 94 (1988).
15. J. H. Cann, A. P. Belperio, V. A. Gostin, C. V. Murray-Wallace, *Quaternary Res.* **29**, 153 (1988).
16. J. Chappell, *Search* **14**, 99 (1983).
17. L. Groube, J. Chappell, J. Muke, D. Price, *Nature* **324**, 453 (1986).
18. A. Goede, P. Murray, R. Harmon, *Artefact* **3**, 139 (1978).
19. S. Bowdler, in *Sunda and Sahul: Prehistoric Studies in Southeast Asia, Melanesia and Australia*, J. Allen, J. Golson, R. Jones, Eds. (Academic Press, London, 1977), pp. 205–246.
20. R. Jones, in *ibid.*, pp. 317–386.

21. I thank the Australian Institute of Aboriginal Studies, La Trobe University, and Australian News Print Mills for supporting the fieldwork and funding the radiocarbon dates.

24 August 1988; accepted 4 January 1989

Scanning Tunneling Microscopy of Uncoated recA-DNA Complexes

M. AMREIN, R. DÜRR, A. STASIAK, H. GROSS, G. TRAVAGLINI*

Uncoated recA-DNA complexes were imaged with the scanning tunneling microscope (STM). The images, which reveal the right-handed helical structure of the complexes with subunits clearly resolved, are comparable in quality to STM images of metal-coated specimens. Possible conduction mechanisms that allow STM imaging of biological macromolecules are discussed.

THE RESOLVING POWER OF THE STM for analyzing structural and electronic properties of metal and semiconductor surfaces is now well established. We have showed that biological specimens coated with a thin conducting film can be analyzed with the STM and that with this technique molecular details can be revealed (*1*). Recent STM work on organic molecules (*2, 3*), adsorbed on a conducting support, extended the possible application of STM to macromolecules classically thought to be insulating. Tunneling on uncoated organic matter with large three-dimensional structure, such as biological macromolecules, has been reported (*4–9*). However, it was necessary that the specimen be coated with a conducting film or replicated (*10*) to obtain a resolution of structural details comparable to that obtainable with the transmission electron microscope (TEM) (*1, 11*). We report that recA-DNA complexes adsorbed from solution onto a salt-coated conducting film and kept humid during measuring can reproducibly yield high-quality STM images.

The recA-DNA complexes were formed in the presence of ATP-gamma-S (the nonhydrolyzable analog of adenosine triphosphate) under conditions that promote the

M. Amrein, R. Dürr, A. Stasiak, H. Gross, Institute of Cell Biology, Swiss Federal Institute of Technology, ETH Hönggerberg, 8093 Zurich, Switzerland.
G. Travaglini, IBM Research Division, Zurich Research Laboratory, 8803 Rüschlikon, Switzerland.

*To whom correspondence should be addressed.

formation of stable complexes (*12*). TEM images of negatively coated specimens (*13*) and STM images of metal-coated specimens (*1*) revealed that under these conditions recA-DNA complexes form right-handed helical filaments with 10-nm diameters, where about six recA protomers contribute to one helical repeat. Formed complexes were purified from unbound recA protein on a Sepharose 2B column and subsequently adsorbed onto platinum-carbon (Pt-C)–coated mica platelets and consequently treated with either magnesium chloride ($MgCl_2$) or magnesium acetate ($MgAc_2$). The Pt-C film was evaporated on freshly cleaved mica to an average thickness of 2 nm at 10^{-6} mbar and room temperature with an electron beam–heated evaporator. After the Pt-C films had been exposed to a glow discharge at 0.1 mbar for 30 s, we coated them with a thin layer of $MgCl_2$ or $MgAc_2$ by putting them on a drop of the respective 5 m*M* salt solution for 1 min. Then the solution was removed and the sample was allowed to dry. For adsorption, films with supporting mica platelets were floated again for 1 min on 5 m*M* $MgCl_2$ drops containing suspended recA-DNA complexes.

The adsorption of recA-DNA complexes on these supports was very dense, as verified by TEM. In the TEM micrographs, very often the filaments seemed slightly embedded in the salt layer. Tunneling was carried out with a pocket-size STM (*14*) under atmospheric conditions. For imaging we used etched gold tips, negatively biased, a tunnel voltage of 300 mV, and a current of 0.5 nA. No polarization or voltage dependence of the images has been observed. The sample had to be kept humid to achieve stable imaging. Therefore, periodically a drop of bidistilled water was put on the sample, and we removed any excess water by blotting the sample with a piece of damp filter paper. During scanning, recA-DNA complexes were frequently moved by the tip; thus they could not be imaged over long distances. This effect was diminished when they were adsorbed in dense arrays. On the other hand, such samples, which are crowded in many regions, made sorting out clean, well-preserved individual filaments difficult in both TEM and STM. Depending on the tip geometry and orientation of the complexes, a tip-sample convolution caused a slightly broadened representation of the filaments.

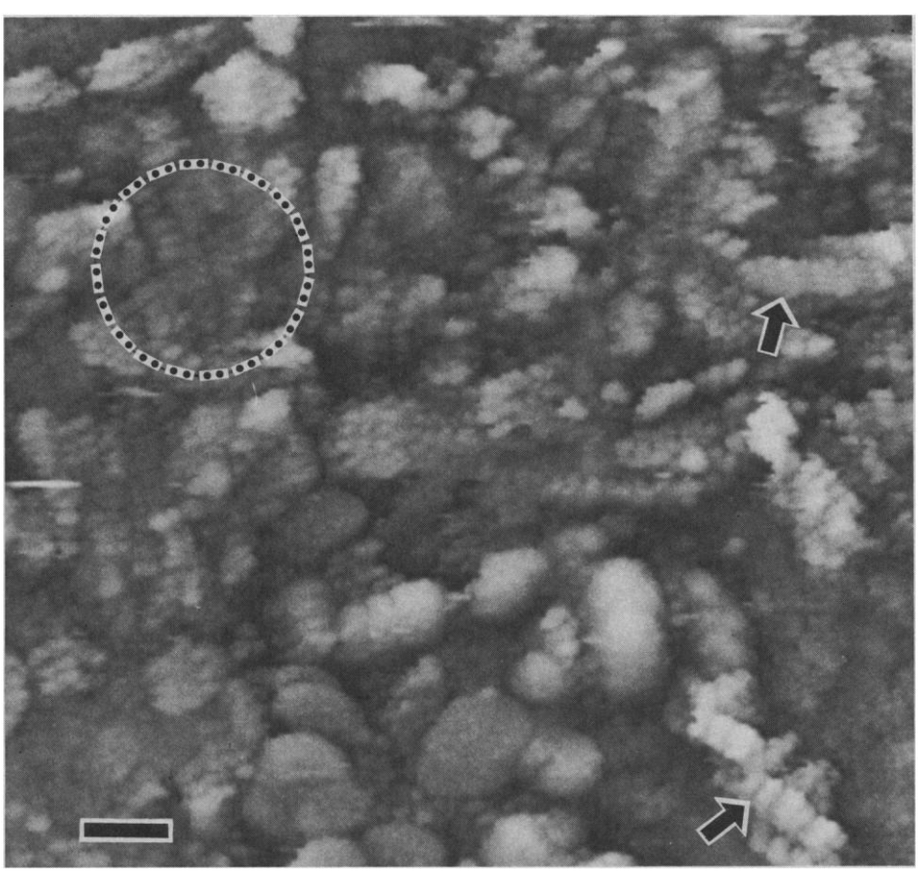

Fig. 1. Low-magnification STM images of uncoated recA-DNA complexes densely adsorbed on a $MgCl_2$-treated Pt-C film. In some regions individual filaments cannot be separated (encircled), although a striation caused by the helical repeat of the structure can easily be distinguished. Single filaments (arrows) show the characteristically right-handed helical structure. The image is a top view in gray-tone representation. Scale bar, 20 nm.

A low-magnification STM image of very densely adsorbed uncoated recA-DNA filaments is shown in Fig. 1. In some regions complexes can barely be separated into individual filaments, even though striations corresponding to the helical repeats of the filaments are well visible. On the right side of Fig. 1, individual complexes can be easily distinguished as characteristic right-handed helical filaments. RecA-DNA complexes in such dense preparations have the tendency to align side by side, and samples prepared in parallel but observed with TEM show similar images of aligned complexes.

A higher magnification image of an individual filament is shown in Fig. 2, where every striation shows a three- to four-part structure. Because this image represents only half of the surface of the helical filament, every helical turn of the complex is composed of about six such parts that presumably are the recA protomers. In some of the visible striations, protomers seem to be composed of two parts that might correspond to different domains of these protomers. The filament shown also has a region where two successive helical repeats are in close contact. These deviations from perfect helical order seem to reflect intrinsic properties of recA-DNA complexes, because they were also observed in STM images of metal-coated preparations of freeze-dried recA-DNA complexes [(*1*); see also the comparison of the two STM imaging methods in Fig. 3].

With the use of this method, features as small as a recA monomer (37,000 daltons) are resolved without any need for averaging. This allows poorly ordered or nonordered structures to be studied with high resolution. Working with humid biological samples allows minimization of structural alterations caused by drying. A first step was made toward tunneling in an aqueous solution (where biological macromolecules remain in the native state) by imaging an uncoated, hydrated sample.

Before we discuss STM imaging of uncoated (naked) macromolecules, let us first consider possible conduction mechanisms in related organic systems, which are better characterized physically, such as polymer chains and the Langmuir-Blodgett films of alkane-tailed molecules, in order to focus on aspects of interest for STM imaging in general.

The electronic structure of such molecular entities is dominated by intramolecular bonds and is essentially unaffected by intermolecular interactions. For saturated backbone polymers without pendant groups,

such as the polyethylene $(CH_2)_n$ alkane tails of Langmuir-Blodgett molecules and lipids, band theory can be applied. The degeneracy of 12 or more molecular orbitals is lifted by the formation of one-dimensional bonding and antibonding bands (*15*). These bands are nevertheless narrow because of the small transfer integral along the chain. This kind of polymer and alkane tail can be considered an organic semiconductor with a large energy gap. The upper valence band formed by carbon $2p$ and hydrogen $1s$ orbitals lies about 9 eV below the vacuum level, whereas the lowest conduction band lies above; electrons injected into the middle of this band have a delocalized nature (*16, 17*).

In the case of saturated backbone polymers with pendant groups, such as polystyrene, the semiconducting-band picture is not valid (*18*). The transfer integral between pendant groups along the chain is so small that their electronic structure remains similar to that of single molecular subunits. Electrons injected into empty states are localized by correlation or disorder as in the Anderson model and are trapped there in the form of charged ions. Dramatic polarization effects caused by such charged radicals occur; intrinsic empty antibonding bulk states close to the vacuum level relax when charged to mid-gap states (*19*), which can be involved in carrier transport along the chain.

Photoinjection experiments (*20*) between metals and nonconducting polymers without intrinsic bulk states established the existence of extrinsic interface states with energies in the forbidden gap. The microscopic nature of such defects is not clear. There are at least four possibilities: (i) specific surface defects, (ii) adsorbed molecules, (iii) products of chemical interactions of the ambient atmosphere with the surface, and (iv) chain end groups (intrinsic). Photoemission experiments (*21*) indicate filled surface states and traps 4 eV below the vacuum level.

Electrical conduction through built-up fatty acid monolayers between metal electrodes has been interpreted in terms of tunneling (*22*) through each whole alkane chain, because intrinsic mid-gap bulk states are not expected. In such experiments, as well as in STM measurements on Langmuir-Blodgett films, the Fermi levels of both metal electrodes or the Fermi levels of the tip and Langmuir-Blodgett support are pinned in the middle of the gap by extrinsic surface states.

In terms of the above-mentioned inorganic semiconductor picture, a Langmuir-Blodgett monolayer represents a potential barrier height of at least 2 eV for tunneling electrons, if we take into account image potential and polarization; band "bending" effects induced by head groups, by extrinsic surface states, and by the proximity of the tip also contribute to a local decrease of the barrier height. We prefer to discuss first the STM contrast mechanism of Langmuir-Blodgett films exposed to ambient conditions in terms of such surface states.

Electrical conduction (*22, 23*) as well as photoinjection experiments (*20*) yield an effective two-dimensional surface state density at the Fermi level of order 10^{14} to 10^{15} eV^{-1} cm^{-2}. Assuming a Mott-type intersite hopping mechanism, a mean hopping distance of 5 Å, and a wave function inverse decay length of 0.35 $Å^{-1}$ parallel to the surface, which corresponds to half of the bulk inverse length extracted from (*23*), we obtain a specific two-dimensional surface resistance of at least 10^8 to 10^9 ohms, which is in the range of STM tunneling resistance (*24*).

Within this solid-state picture and considering the hopping mechanism alone, STM imaging of Langmuir-Blodgett films is possible only in the neighborhood of extended defects or internal surfaces (for a multilayer assembly or a lipid membrane), which electrically connect the scanned surface to the conducting support. Moreover, fast electron transfer through the molecule may occur. In contrast to the electrical conduction experi-

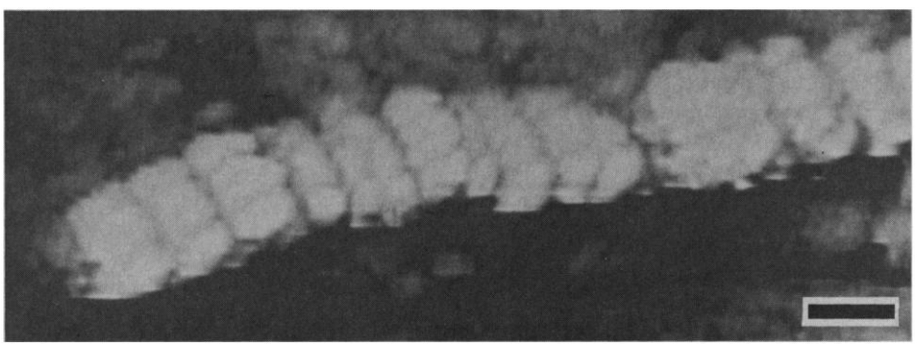

Fig. 2. STM image of an individual, uncoated recA-DNA complex adsorbed on a $MgAc_2$-treated Pt-C film. A long-range corrugation of the supporting film and local distortions were eliminated by reconstruction and subtraction of the deformed support surface with the use of elastic models (*29*). Every striation, corresponding to one helical turn, is composed of three to four radially repeating parts. Such substructures seem to represent the recA protomers. Scale bar, 10 nm.

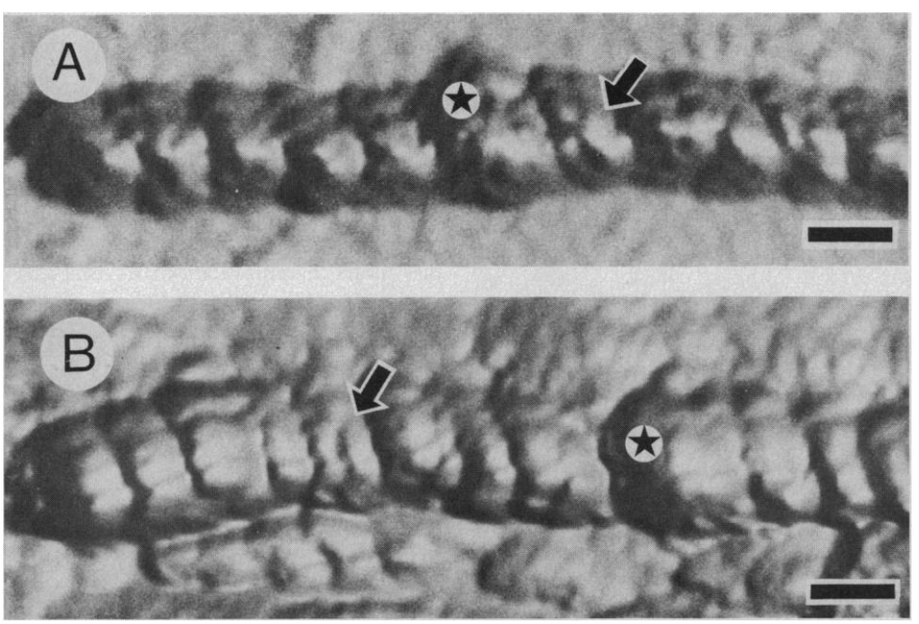

Fig. 3. Comparison of STM images of (**A**) a freeze-dried and metal-coated recA-DNA complex and (**B**) the uncoated complex of Fig. 2. The images are presented as top views with simulated shading and enhanced filament structures. The characteristic features appear in good agreement for the two methods, giving confidence in the reproducibility of STM imaging of such largely corrugated specimens. In both cases the striations are composed of three to four parts, corresponding to recA protomers. However, they are better resolved on the uncoated sample. In some cases radially repeated parts seem to consist of two domains (arrows). Both filaments also have a region where two successive striations are in close contact (asterisks). Scale bar, 10 nm.

ments, no oxidized support was used in the STM experiments on Langmuir-Blodgett films. Furthermore, the system under consideration is not a single molecule alone but a molecule between the two electrodes, that is, the tip and support. A coupling with the electrodes can modify the electronic structure of the single molecules and thus affect their transmission (*25*). Generally, interactions with molecular vibrations (normally weakly dispersive) and molecular polarization can strongly affect the electronic wave function overlap and thus the electronic energies. The parameters that govern electron propagation in organic materials are different from those that operate in inorganic compounds. Time-dependent energy states, polarization terms, and electron-electron interactions must be considered in order to explain electron transfer in organic solids.

Finally, let us consider the possibility of electrical breakdown. In STM experiments the voltage between tip and sample is in the range of a few hundred millivolts, which corresponds to an electrical field strength of the order of 0.2 mV cm^{-1} if we assume that the voltage drops linearly across the entire Langmuir-Blodgett monolayer. This field strength corresponds to the typical breakdown strength of an 80-μm-thick multilayer (*26*), but for mono- and bilayers larger electric fields are required. In addition, for electrical breakdown large electronic energies are required in processes for carrier multiplication (*27*). In contrast, the energies involved in STM experiments are very small; Zener tunneling can thus be excluded. Energy-loss processes of tunneling electrons are negligible for breakdown.

A microscopic description of the imaging of a recA-DNA complex, an extremely complicated system, requires detailed knowledge of the physical properties of its single components and their interactions. The considerations about the pendant-group polymers might also be valid for polypeptide chains, which can be regarded as biological polymers with residues acting as pendant groups. Proteins are highly structured macromolecules: their specific structure will also influence the quantum paths, controlling whether long-range electron transfer occurs (*28*).

STM imaging of recA-DNA complexes required treating the Pt-C supporting film with $MgCl_2$ or $MgAc_2$ solution and keeping the samples wet. The recA-DNA filaments are therefore embedded in a strongly polar medium, which can also act as an electrolyte. The exact role of the salt solution is not yet clear. The fluctuations of the surrounding medium and its polarization changes can locally and temporally shift the electronic terms of the macromolecule and its hydration shell. Long-range electron transfer can thus be induced by polarization energy effects in the macromolecule, and in the hydration shell itself through nonequilibrium states of molecular subunits and solvated ions. Electrochemical processes probably contribute to imaging and also influence the contact resistance between object and support. Ionic conductivity can be excluded owing to the small mobility of ions in water (10^{-4} cm^2 V^{-1} s^{-1}). Also, Mg^{2+}, Cl^-, and Ac^- could act as dopants of the macromolecule, thus providing the charge transfer necessary for electron transfer.

REFERENCES AND NOTES

1. M. Amrein, A. Stasiak, H. Gross, E. Stoll, G. Travaglini, *Science* **240**, 514 (1988).
2. J. K. Gimzewski, E. Stoll, R. R. Schlittler, *Surf. Sci.* **181**, 267 (1987).
3. J. S. Foster and J. E. Frommer, *Nature* **333**, 542 (1988).
4. A. M. Baro *et al.*, *ibid.* **315**, 253 (1985).
5. A. Stemmer *et al.*, *Surf. Sci.* **181**, 394 (1987).
6. S. M. Lindsay and B. Barris, *J. Vac. Sci. Technol. A* **6**, 544 (1988).
7. G. Travaglini *et al.*, *Phys. Scr.* **38**, 309 (1988).
8. D. P. E. Smith *et al.*, *Proc. Natl. Acad. Sci. U.S.A.* **84**, 969 (1987).
9. H. Fuchs, *Phys. Scr.* **38**, 264 (1988).
10. J. A. N. Zasadzinski, J. Schneir, J. Gurley, V. Elings, P. K. Hansma, *Science* **239**, 1013 (1988).
11. R. Guckenberger *et al.*, *Ultramicroscopy* **25**, 111 (1988).
12. A. Stasiak, E. Di Capua, Th. Koller, *J. Mol. Biol.* **151**, 557 (1981).
13. E. H. Egelman and A. Stasiak, *ibid.* **191**, 677 (1986).
14. C. Gerber, G. Binnig, H. Fuchs, O. Marti, H. Rohrer, *Rev. Sci. Instrum.* **57**, 221 (1986).
15. J. J. Pireaux *et al.*, *Phys. Rev. A* **14**, 2133 (1976).
16. K. Seki, N. Ueno, U. O. Karlsson, R. Engelhardt, E. E. Koch, *Chem. Phys.* **105**, 247 (1986).
17. A. Karpfen, *J. Chem. Phys.* **75**, 238 (1981).
18. C. B. Duke *et al.*, *Phys. Rev. B* **18**, 5717 (1978).
19. C. B. Duke and T. J. Fabish, *Phys. Rev. Lett.* **16**, 1075 (1976).
20. T. Mizutani, Y. Takai, T. Osawa, M. Ieda, *J. Phys. D* **9**, 2253 (1976).
21. Y. Murata, *Jpn. J. Appl. Phys.* **18**, 1 (1979).
22. B. Mann and H. Kuhn, *J. Appl. Phys.* **42**, 4398 (1971).
23. M. Sugi, T. Fukui, S. Ilzima, *Chem. Phys. Lett.* **45**, 163 (1977).
24. The method in (*22*) yields for a Langmuir-Blodgett molecule a resistance of 10^{24} ohms, 15 orders of magnitude larger than the STM gap resistance.
25. P. Sautet and C. Joachim, *Chem. Phys. Lett.*, in press.
26. K. Yoshino, S. Harada, J. Kyokane, Y. Inuishi, *J. Phys. D* **12**, 1535 (1979).
27. E. Cartier and P. Pfluger, *Phys. Rev. B* **34**, 8822 (1986).
28. A. Kuki and P. G. Wolynes, *Science* **236**, 1647 (1987).
29. R. Dürr, thesis, Swiss Federal Institute of Technology, Zurich (1988).

30. We thank A. Baratoff, D. Baeriswyl, and H. Rohrer for stimulating discussions and for reading the manuscript.

8 November 1988; accepted 17 January 1989

Upper Jurassic Dinosaur Egg from Utah

KARL F. HIRSCH, KENNETH L. STADTMAN, WADE E. MILLER, JAMES H. MADSEN, JR.

The Upper Jurassic egg described here is the first known egg from the 100-million-year gap in the fossil record between Lower Jurassic (South Africa) and upper Lower Cretaceous (Utah). The discovery of the egg, which was found mixed in with thousands of dinosaur bones rather than in a nest, the pathological multilayering of the eggshell as found in modern and fossil reptilians, and the pliable condition of the eggshell at the time of burial indicate an oviducal retention of the egg at the time of burial.

A NEARLY COMPLETE EGG WAS found in September 1987 in the Cleveland-Lloyd Dinosaur Quarry at a site located in the lower fossiliferous beds of the Brushy Basin Member of the Upper Jurassic Morrison Formation in Emery County, east central Utah (*1*). This quarry has yielded more than 12,000 disarticulated bones representing 70 or more individuals of at least 12 dinosaur genera (*1–4*). In the Late Jurassic, this area may have been a shallow lake or marsh where the animals became trapped in mud (*4*).

The egg was found embedded in a calcareous blocky shale 0.4 m above the bottom of the fossiliferous stratum in the quarry. The fossil was not immediately associated with skeletal parts of the dinosaurs, although disarticulated remains of the sauropods *Barosaurus* and *Camarasaurus* and *Stegosaurus* were nearby. There was a concentration of a single theropod, *Allosaurus*, including sacral and appendicular elements, in the vicinity of the egg. *Allosaurus* is by far the most abundant taxon in the Cleveland-Lloyd dinosaur fauna. It cannot be demonstrated that the egg represents any of the above genera. No additional eggshell material was found.

The preservation and condition of the egg make it unlikely that it was transported. The

K. F. Hirsch, University of Colorado Museum, Campus Box 218, Boulder, CO 80309.
K. L. Stadtman and W. E. Miller, Geology Department, Brigham Young University, Provo, UT 84602.
J. H. Madsen, Jr., 1814 East 3900 South, Salt Lake City, UT 84124.